# Electrical Conductivity Versus Temperature in Freezing Conditions: A Field Experiment Using a Basket Geothermal Heat Exchanger

A Coperey, A Revil, B Stutz

Geophysical Research Letters

RESEARCH LETTER
10.1029/2019GL084962

**Key Points:**
- Electrical conductivity is related to temperature via a soil freezing curve
- Frozen ground is generated in the field using a geothermal heat exchanger
- Both field and laboratory experiments are consistent with the theory

**Correspondence to:**
A. Revil,
andre.revil@univ-smb.fr

**Citation:**
Coperey, A., Revil, A., & Stutz, B. (2019). Electrical conductivity versus temperature in freezing conditions: A field experiment using a basket geothermal heat exchanger. *Geophysical Research Letters*, *46*. https://doi.org/10.1029/2019GL084962

Received 12 AUG 2019
Accepted 11 NOV 2019
Accepted article online 4 DEC 2019



# Electrical Conductivity Versus Temperature in Freezing Conditions: A Field Experiment Using a Basket Geothermal Heat Exchanger

**A. Coperey[1,2], A. Revil[3], and B. Stutz[2]**

[1]Université Grenoble Alpes, Université Savoie Mont Blanc, CNRS, IRD, IFSTTAR, ISTerre, Grenoble, France, [2]LOCIE, Université Savoie Mont-Blanc, CNRS, UMR5271, Chambéry, France, [3]Université Grenoble Alpes, USMB, CNRS, EDYTEM, Chambéry, France

**Abstract** We use a basket geothermal heat exchanger during 518 hr to freeze a portion of soil. This field experiment is monitored using time lapse electrical conductivity tomography and a set of 47 in situ temperature sensors. A frozen soil core characterized by negative temperatures and low conductivity values ($<10^{-3}$ S/m) develops over time. A petrophysical model describing the temperature dependence of the electrical conductivity in freezing conditions is applied to the field data and compared to two laboratory experiments performed with two core samples from the test site. The results show that this petrophysical model can be used to interpret field measurements bridging electrical conductivity to temperature and liquid water content.

**Plain Language Summary** In order to better understand the evolution of permafrost (spatial extent, temperature, and liquid water content distributions), we can use time lapse electrical conductivity tomography. The electrical conductivity of a soil is influenced by water and ice contents, temperature, salinity of the pore water, and the cation exchange capacity of the material. We test a physics-based relationship connecting temperature, ice content, and electrical conductivity. This relationship is tested on two core samples and compared with field observations during a in-situ test experiment. In this experiment, we generated a frozen soil core using a geothermal heat exchanger, and at the same time, we recorded the temperature and electrical conductivity distributions. We found a good consistency between the field data and the model, which means that from the distribution of the electrical conductivity of the frozen soil, we are able to recover its temperature.

## 1. Introduction

There are several reasons to develop techniques able to monitor permafrost in the subsurface of the Earth. First, due to climatic changes, the progressive degradation of permafrost poses a risk to infrastructures (Gruber et al., 2004; Ravanel et al., 2017; Beniston et al., 2018). Monitoring changes in temperatures and ice and liquid water contents in the ground is necessary to understand the adaptation of ecosystems of cold regions and to try to mitigate the release of $CO_2$ into the atmosphere (Schaefer et al., 2014). In addition, anticipating the evolution of permafrost will make it possible to optimize the use of newly available natural resources (Gautier et al., 2009; Instanes et al., 2016). Finally, harvesting thermal energy from the ground to heat buildings and various types of facilities can locally generate frozen areas in the ground that need to be monitored as well (Moch et al., 2015; Self et al., 2013).

Electrical conductivity tomography is a simple geophysical technique that can be used to image and monitor changes in the electrical conductivity distribution of the subsurface. Electrical conductivity tomography has been recently used to image permafrost in the shallow subsurface (e.g., Scott et al., 1990; Kneisel, 2006; Magnin et al., 2015). This has prompted the recent development of an improved physics-based petrophysical model, beyond the classical Archie's law, to connect electrical conductivity to temperature (e.g., Coperey et al., 2019; Duvillard et al., 2018). Such model needs to be further tested. This is the goal of this paper: to precisely test a model connecting electrical conductivity to temperature through an exponential soil freezing curve.

In the present paper, we use a basket heat exchanger to freeze a portion of the ground, which is monitored using time lapse electrical conductivity tomography. This allows reconstructing an in situ electrical

conductivity/temperature relationship, which can be compared to laboratory experiment performed on two core samples from the test site. In turn, these data can be used to test the petrophysical model recently developed by Duvillard et al. (2018) and Coperey et al. (2019).

## 2. Electrical Conductivity Versus Temperature

In the absence of ice in the pore space, the dependence of the electrical conductivity of a soil $\sigma(T)$ (in S/m) with the temperature $T$ is given by (Vinegar & Waxman, 1984)

$$\sigma(T) = \sigma(T_0)[1 + \alpha_T(T - T_0)], \tag{1}$$

where $\alpha_T \approx 0.021\ °C^{-1}$, $T_0 = 25$ °C. Fundamentally, equation (1) reflects the effect of temperature on the ionic mobility of the charge carriers. Below the freezing temperature, we need to consider the change in the liquid water content $\theta$ (dimensionless) with temperature $T$ and the segregation of the salt in the liquid pore water. The following freezing curve can be used to describe the dependence between $\theta$ and $T$ (in °C) (see Duvillard et al., 2018):

$$\theta(T) = \begin{cases} (\phi - \theta_r)\exp\left(-\dfrac{T - T_F}{T_C}\right) + \theta_r, T \leq T_F \\ \phi, T > T_F \end{cases}, \tag{2}$$

where $T_F$ (in °C) denotes the freezing temperature, $T_C$ (in °C) denotes a characteristic temperature associated to the pore size distribution, $\theta_r$ denotes the residual liquid water content at low temperatures, and $\phi$ (dimensionless) denotes the (connected) porosity. The soil freezing curve can be related to the characteristics of the pore size distribution like the capillary pressure curve (Spans & Baker, 1996). In freezing conditions and accounting for the salt segregation effect, the electrical conductivity of the porous material is (Coperey et al., 2019)

$$\sigma(T) = \sigma(T_0)[1 + \alpha_T T - T_0], \tag{3}$$

where $m$ (dimensionless) corresponds to the porosity exponent of Archie's law and $\sigma(T_0)$ denotes the conductivity (in S/m) at the reference temperature $T_0$ (=25 °C). While not apparent in equation (3), this model comprises both a conductivity contribution in the pore space and a surface conductivity contribution associated with electrical double layer (and therefore related to the cation exchange capacity [CEC] of the material). Assuming $m \approx 2.0$ (Vinegar & Waxman, 1984) and using equations (2) and (3), the conductivity of a soil depends on the temperature according to

$$\sigma(T) \approx \left[(\phi - \theta_r)\exp\left(-\frac{T - T_F}{T_C}\right) + \theta_r\right]\frac{\sigma(T_0)}{\phi}[1 + \alpha_T(T - T_0)]. \tag{4}$$

Equation (4) has been developed for fully liquid water-saturated conditions above the freezing temperature. It can be easily generalized to conditions for which the initial water content is $\theta_i$ (rather than the water content at saturation $\theta_S = \phi$) by replacing $\phi$ by $\theta_i \leq \phi$ in equation (4). In the present study, we want to test these equations to model the change in conductivity associated with freezing of a soil.

## 3. Field Experiment

Five helical geothermal heat exchangers were set up in 2011 (labelled HE1 to HE5) at a test site located in Technolac in Savoie, France. HE1 is made of 100 m of polyethylene tube (internal/external radii 25 and 22.7 mm, respectively), enrolled with a pitch of 0.08 m (Figure 1). They were buried at a depth of 3.4 m and backfilled by the local soils and sediments with a mix of clay, silt, and gravels. They are located in the vadose zone of the soil above the water table, located roughly at a depth of 5 m. The circulating fluid is a monopropylene glycol aqueous solution (40% glycol in weight) for the heat exchangers, and water is used for the convector heaters. For our experiment, we used two heat exchangers. The activity of HE1 is monitored using electrical conductivity tomography (Figure 1). HE5 (located 20 m away from HE1) is used to adjust mass flow for a correct functioning of the heat pump.

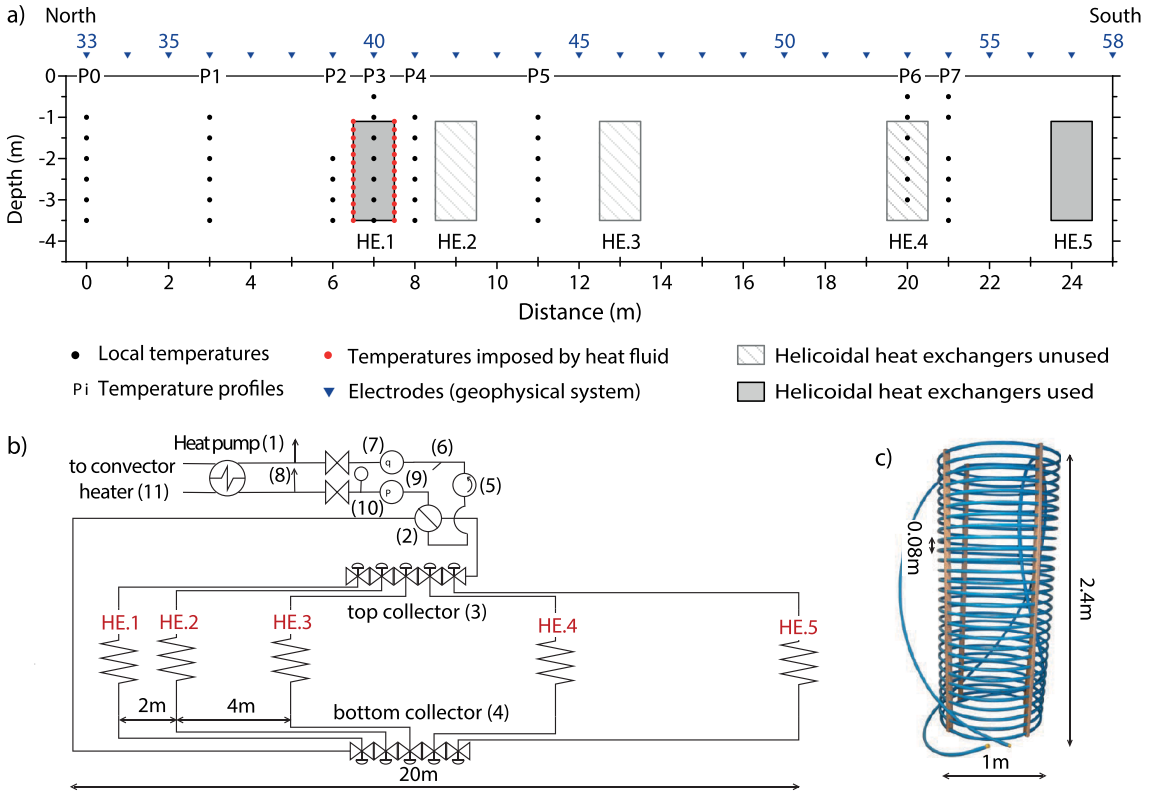


**Figure 1.** Sketch of the geometrical setup used for the field experiment. (a) Geometrical setup of heat exchangers and temperature probes. The test site comprises five basket heat exchangers (labelled HE1 to HE5, Terra Spiral exchangers) buried between 1.1 and 3.5 m. During the experiment, only two heat exchanges are used, and we focus our experiment on HE1. The temperature distribution around HE1 is monitored with 47 thermocouples, distributed along seven vertical profiles (labelled P0 to P7). In addition, the temperatures of the soil in contact with the spires of HE.1 are determined from the inlet/outlet temperature on the heat-carrying fluid (see the red dots on HE1). Along the ground surface, we use 64 stainless steel electrodes (only electrodes 33 to 58 are shown, blue arrows) with a spacing of 1.0 m to perform a 2.5-D electrical conductivity tomography. (b) Description of the main components of the geothermal heat pump. (HE) Terra Spiral exchangers (from Ryb); (1) heat pump (AUREA 20Z from Ciat); (2) four-way valves; (3, 4) heat exchanger selecting valves; (5) circulatory pumps; (6) filter; (7) flow meter; (8) steam traps; (9) manometers; (10) expansion tank; (11) convector heater (MAJOR 2 from Ciat). (c) Helical heat exchanger. The coil corresponds to 100 m of a polyethylene.

Before starting the heat pump, we recorded the background temperature of the soil during 96 hr. At $t = 0$ hr, we started the heat pump and the circulator pumps, which worked for 518 hr (≈21.6 days). Data measurements (soil and fluid temperatures, mass flows, and extracted heat) was performed every 15 min (Figure 2). We recorded ground temperatures along seven vertical profiles thanks to four wire Pt100 probes with an accuracy of 0.2 °C (Figures 1a and 3). We also used the temperature along the heat exchanger tube to improve our estimate of the ground temperature distribution. Snapshots of the temperature distributions are shown in Figure 3.

In addition of temperature measurements, we performed electrical conductivity tomography. We took nine snapshots of electrical conductivity measurements along a single profile before and after the heat pump was turned on. The measurement times are $t_1 = -22$ hr, $t_2 = 0$ hr, $t_3 = 22$ hr, $t_4 = 48$ hr, $t_5 = 74$ hr, $t_6 = 146$ hr, $t_7 = 194$ hr, $t_8 = 242$ hr, and $t_9 = 518$ hr. The measurements were performed with an ABEM-SAS Terrameter and 64 steel electrodes (spacing 1.0 m, see position in Figure 1a). We used a Wenner protocol, and the number of stacks was between 3 and 6 to target a standard deviation of of less than 1%. The nine pseudosections data were inverted with the software IP4DI using the time lapse inversion approach developed by Karaoulis et al. (2013). In order to improve inversion, we used a nonuniform time regularization called the Active Time Constrained method (Karaoulis et al., 2014). The inversion converged at Iteration 8 for which the root-mean-square error reaches a constant level. To highlight the resistivity anomaly resulting from temperature variations, we computed the change in model resistivity for each snapshot with respect to the background section (Figure 3).

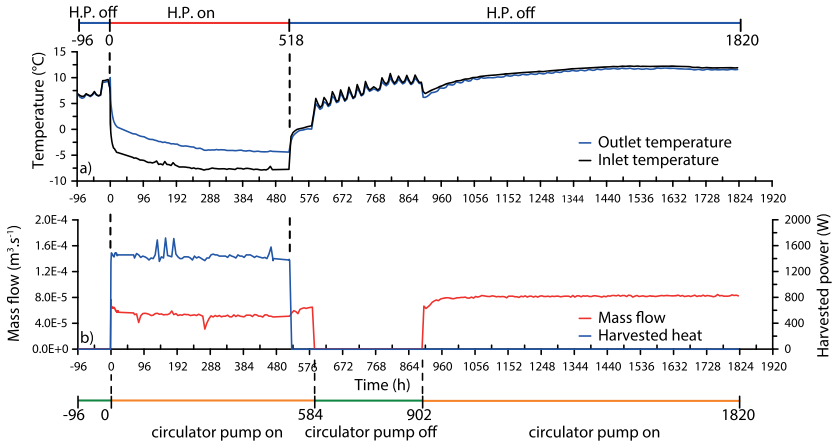


**Figure 2.** Experimental setup. (a) Entrance and exit temperatures. The heat pump (HP) and circulator pumps were started at $t = 0$ hr, during 518 hr (≈21.6 days). After only 1 hr of running, the temperature of the heat-carrying fluid entering by the bottom of the heat exchanger was below 0 °C. After ~35 hr, the exit fluid temperature was also below 0 °C. Just before the heat pump stops ($t = 518$ hr), entrance and exit fluid temperatures were −7.2 and −3.0 °C, respectively. (b) Heat extracting and mass flow for the heat exchanger HE1. During this stage, the heat extracting and mass flow oscillated around 722 W and $5.45 \cdot 10^{-5}$ m$^3$/s, respectively. At $t = 518$ hr, the heat pump was switched off, and the exit fluid reached 0 °C after 24 hr. The circulator pumps were stopped at 584 hr.

## 4. Results and Interpretations

### 4.1. Field Experiment

In Figure 3, we see that the temperature distribution around the heat exchanger decreases to negative values indicating that the area, in the presence of liquid water, is susceptible to freeze. Simultaneously, the resistivity increases drastically in the upper part of the heat exchanger where liquid water is likely to be present. In

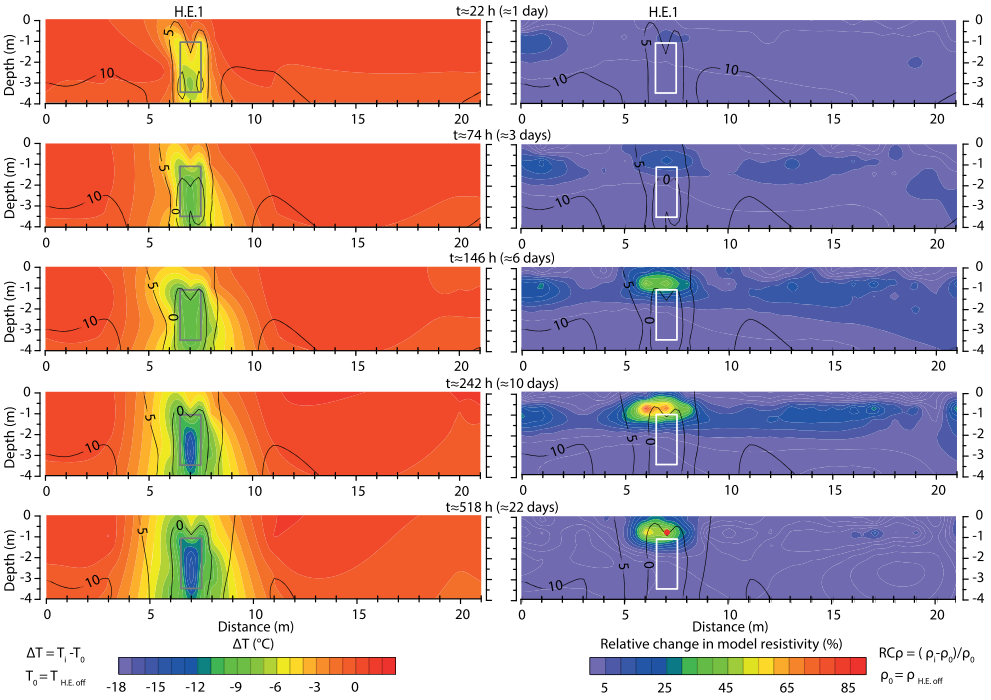


**Figure 3.** Snapshots of the temperature change and relative change in resistivity distributions for five selected times. The contour lines denote the temperature in °C. The position of the heat exchanger HE1 is also shown on the sections. The reference time ($t_0$) corresponds to the acquisition performed when the heat pump started. The red dot on the last section denotes the position at which electrical conductivity is reported as a function of temperature in Figure 4.

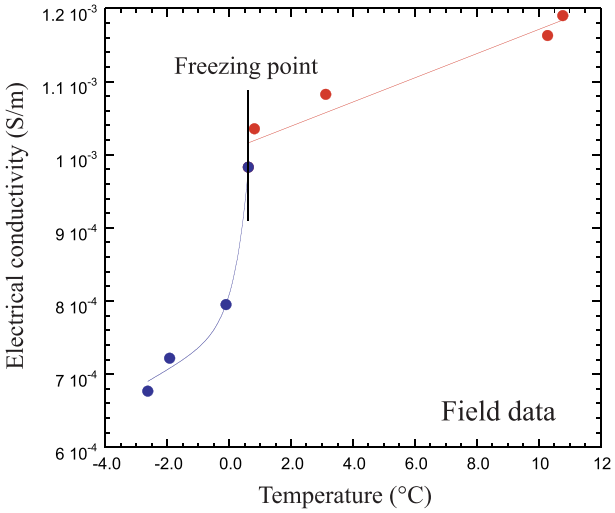


**Figure 4.** Electrical conductivity versus temperature from the in situ measurement. The symbols denote the field data (red above the freezing temperature and blue below the freezing temperature), while the plain lines correspond to the fit of the model. The model discussed in the text fits the data relatively well. We need to remember that the initial water content is close to the residual water saturation. This explains the relatively modest change in the conductivity during freezing conditions. In other words, the results imply that the material is already pretty dry when freezing starts. Above the freezing point, the model parameters are $\sigma(T_0 = 25\ ^\circ\text{C}) = (1.42 \pm 0.05) \times 10^{-3}$ S/m and $\alpha_T = 0.012 \pm 0.002/^\circ\text{C}$ ($r^2 = 0.93$). Below the freezing point, the value of model parameters are $T_C = -0.46 \pm 0.16$ °C, $\theta_i = 0.010 \pm 0.007$, and $\theta_r = 0.0014 \pm 0.0003$ ($r^2 = 0.99$). The freezing point is slightly above 0 °C. This positive temperature can be explained by the uncertainty in the interpolation of the temperatures from the point measurements.

order to better analyze the resistive anomaly, we extracted the electrical conductivity data at position P3 (depth of 0.8 m) for the snapshots shown in Figure 3. These conductivity data are reported as a function of temperature in Figure 4. We need to remember that the soil at the position of the heat exchanger is not fully water saturated. Consequently, the initial value of the water content is much below the value of the porosity (dry soil). We use equations (1) and (4) to fit the data shown in Figure 4. The values of the fitting parameters are $\theta_r = 0.001$, $T_c = -0.76$ °C, and $\theta_i = 0.002$ (see Table 1).

### 4.2. Comparison With Laboratory Experiments

In order to further test the relationship between electrical conductivity and temperature, we use two soils from the test site labeled SW and NW. Their CEC and porosity are reported in Table 1. The two experiments were performed in a temperature-controlled bath. The samples were first dried and then saturated under vacuum with pore water from the aquifer. The electrical conductivity of this water was measured with a calibrated conductimeter (0.117 S/m at 27 °C). The temperature-controlled bath is a KISS K6 chamber from Huber working with a precision of 0.1 °C in the temperature range −16 to +20 °C. The electrical conductivity measurements were performed with the impedance meter developed by Zimmermann et al. (2008) and are reported here at 1 Hz. The experimental data together with a fit of the data with equations (1) and (4) are shown in Figure 5. We see that the model fits the data for all the temperature investigated here. In Table 1, we see that the model parameters are consistent between the field and laboratory experiments. We have to remember that the main difference between the field and laboratory experiment corresponds to the initial water content. Indeed, the modeling from Figure 4 indicates that the soil is nearly dry when the freezing begins, which explains the reduced variations in resistivity in the time lapse tomograms.

## 5. Discussion

In the field experiment, we need to explain why the variation in the electrical conductivity is limited to the shallow subsurface (first meter). It is known that the formation of ice in a porous material sucks the liquid water through capillary pressure effects (cryosuction) and could have dried up the soil around the frozen soil core. This effect has been described in the literature (e.g., Sass, 2004, and references therein). Another effect is that the heat exchanger could mask the resistivity variations at its position.

Another point that needs to be discussed is the uncertainty associated with the model parameters determined from a least squares technique. These parameters are very well constrained by the data. For instance,

**Table 1**
*List of the Optimized Parameters for the In-Phase Conductivity*

| Experiment | $\sigma(T_0)$ | $\alpha_T$ | $\theta_r$ | $T_c$ | CEC | $\phi$ |
|---|---|---|---|---|---|---|
| In situ | 0.0014 | 0.012 | 0.001 | $-0.5 \pm 0.2$ | — | — |
| Sample NW | 0.039 | 0.017 | 0.003 | $-2.3 \pm 0.1$ | $8.7 \pm 1.0$ | $0.21 \pm 0.01$ |
| Sample SW | 0.0017 | 0.019 | 0.002 | $-2.3 \pm 0.1$ | $10.1 \pm 1.0$ | $0.23 \pm 0.01$ |

*Note*. The conductivity $\sigma(T_0)$ and the residual conductivity $\sigma_r(-10\ ^\circ\text{C})$ are reported in S/m. The sensitivity coefficient $\sigma(T_0)$ is expressed in $^\circ\text{C}^{-1}$ and determined above the freezing condition using the linear models. The residual water content $\theta_r$ is dimensionless, and CEC is the cation exchange capacity in meq/100 g (=963.20 C/kg), and $\phi$ denotes the connected porosity (dimensionless). The fitting was done by considering $m \approx 2$. The initial water contents are respectively equal to 0.002 for in situ experiment and equal to the porosity for the laboratory measurements, which are done in saturated conditions. The critical temperature $T_c$ is associated with the pore size distribution. Note that the fine structure of the two soil samples has not been preserved, and it is therefore not surprising that this parameter is different for the laboratory experiment and for the field experiment.

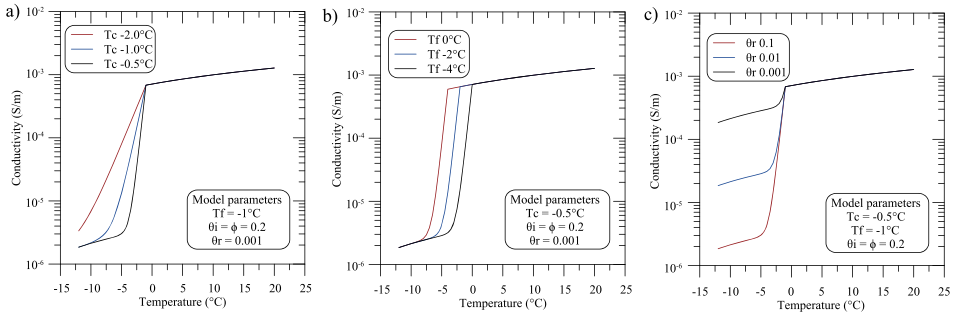


**Figure 5.** Electrical conductivity data versus temperature for two soils samples from the test sites and fit of the data with equation (4). (a) Sample NW between −16 and +20 °C ($T_F = -2.5$ ° C). (b) Soil sample SW between −16 and +20 °C ($T_F = -2.5$ ° C). The value of the model parameters are reported in Table 1. In both cases, the symbols denote the experimental data (red above the freezing temperature and blue below the freezing temperature), while the plain lines correspond to the fit of the model. Compared to the previous figure, we prefer to plot in log scale for electrical conductivity since the change in conductivity is large (more than a decade). The variations in conductivity are greater in these two experiments than in the in situ experiment. This is explained by the different initial saturation. The core sample is fully saturated in the laboratory experiment, while the soil is partially saturated in the field. Note the samples have been remolded, which can explain why the value of $T_C$ is different between the field data and the core samples.

the freezing point is the point where the resistivity exhibits an abrupt drop in the slope of the conductivity versus temperature trends (see Figures 4 and 5). The characteristic temperature defines the abruptness of the transition between liquid and frozen water. The initial water content is related to the magnitude of the drop in resistivity. The residual water content is determined by the plateau of the electrical conductivity level at low temperatures. The characteristic temperature is associated with the pore size distribution. Freezing begins in the large pores, and then, with the decrease in temperature, it can be carried out in smaller pores. This process is very similar to the soil drainage process (Spans & Baker, 1996). The characteristic temperature from the laboratory experiments is close but slightly lower than that determined for the in situ experiment (maximum deviation less than 0.5 °C). Thus, from our point of view, the differences in values are related to the different shapes of temperature curve, induced by different pore size distribution due to their sampling and saturation. In addition, in laboratory measurements, the sample is saturated and releases latent heat that dissipates slowly, whereas in the in situ experiment, the medium is not fully saturated and the latent heat is quickly captured and dissipated thanks to the geothermal exchanger. These differences in dynamics necessarily have an impact on the thermodynamic equilibria and therefore the propagation of the freezing. The sensitivity of these three parameters on the evolution of electrical conductivity versus temperature curve is shown in Figure 6.

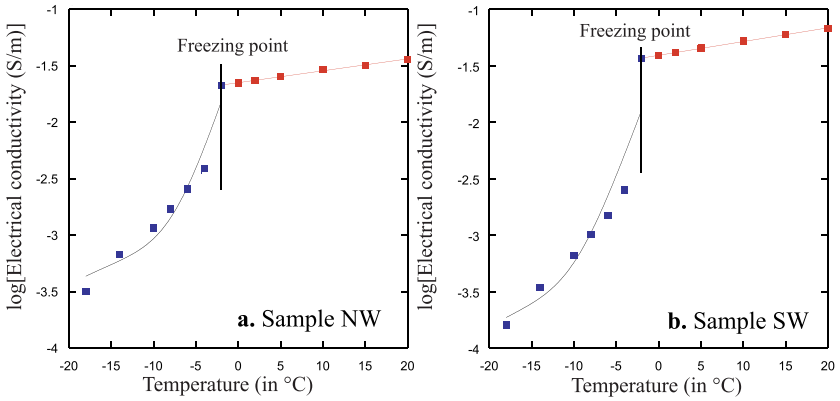


**Figure 6.** Sensitivity study of the electrical conductivity versus temperature for different values of characteristic temperature, freezing point, initial and residual water contents using the freezing curve model corresponding to equation (4). **a.** Influence of the characteristic temperature. **b.** Influence of the freezing point. **c.** Influence of the residual water content. For the part without freezing, the conductivities were computed with equation (1) associated to $\alpha_T$=0.02/°C and $\sigma(T_0 = 25\ ^\circ\text{C}) = 1.42{\cdot}10^{-3}$ S/m.

Other models have been developed in the past to account for the effect of the temperature on the electrical conductivity curve (see, for instance, Minsley et al., 2015; Ren & Kalscheuer, 2019). However, our model is the first to account simultaneously for a number of effects (shown in Figure 6) including (1) the effect of the temperature on the ionic mobility of the charge carriers, (2) a soil freezing curve and its effect on the relationship between temperature and the liquid water content, and (3) the residual water saturation and the effect of the salt segregation. For all these reasons (discussed in detail in Duvillard et al., 2018, and Coperey et al., 2019), our model has a unique way to capture the effect of temperature on the electrical conductivity of porous media and predicts a dependence on the liquid water content that is very different from Archie's law alone, which is unfortunately broadly used in the literature as a conductivity equation without accounting for the effect of surface conductivity and salt segregation.

## 6. Conclusion

We have developed a field experiment using a basket geothermal heat exchanger to generate frozen ground in the shallow subsurface, above the water table. The development of this frozen area was performed using time lapse electrical conductivity tomography, and temperature was monitored using in situ thermal probes combined with the record of the temperature of the heat-carrying fluid in the heat exchanger. The variation of the electrical conductivity with temperature can be understood using a petrophysical model that combined recently developed electrical conductivity models with a soil freezing curve taking the form of an exponential relationship between the water content and the temperature. This is the first time that this model is validated through an in situ experiment and on core samples from the test site. The field data are favorably compared with laboratory measurements; the differences can be explained by different initial water saturation. In the future, we plan to improve the resolution of the electrical conductivity monitoring in order to obtain the temperature field distribution only from the geophysical data.

**Acknowledgments**
We thank A. Soued Ahmed and F. Lavoué for useful discussions about inversion and S. Roque and J. Grangeon for their help in the field. We thank also D. Cloe for his technical support regarding the temperature probes and the heat exchanger. The PhD thesis of A. Coperey is funded by AGIR-POLE-PAGE 2016. The data used in this manuscript are available with DRYAD (https://doi.org/10.5061/dryad.0p2ngf1w2). We thank the Editor and the referees for their useful comments and their time.

## References

Beniston, M., Farinotti, D., Stoffel, M., Andreassen, L. M., Coppola, E., Eckert, N., et al. (2018). The European mountain cryosphere: A review of its current state, trends, and future challenges. *The Cryosphere*, *12*, 759–794. https://doi.org/10.5194/tc-12-759-2018

Coperey, A., Revil, A., Abdulsamad, F., Stutz, B., Duvillard, P. A., & Ravanel, L. (2019). Low frequency induced polarization of porous media undergoing freezing: Preliminary observations and modeling. *Journal of Geophysical Research: Solid Earth*, *124*, 4523–4544. https://doi.org/10.1029/2018JB017015

Duvillard, P. A., Revil, A., Qi, Y., Soueid Ahmed, A., Coperey, A., & Ravanel, L. (2018). Three-dimensional electrical conductivity and induced polarization tomography of a rock glacier. *Journal of Geophysical Research: Solid Earth*, *123*, 9528–9554. https://doi.org/10.1029/2018JB015965

Gautier, D. L., Bird, K. J., Charpentier, R. R., Grantz, A., Houseknecht, D. W., Klett, T. R., et al. (2009). Assessment of undiscovered oil and gas in the Arctic. *Science*, *324*(5931), 1175–1179. https://doi.org/10.1126/science.1169467

Gruber, S., Hoelzle, M., & Haeberli, W. (2004). Rock-wall temperatures in the Alps: Modelling their topographic distribution and regional differences. *Permafrost and Periglacial Processes*, *15*, 299–307. https://doi.org/10.1002/ppp.501

Instanes, A., Kokorev, V., Janowicz, R., Bruland, O., Sand, K., & Prowse, T. (2016). Changes to freshwater systems affecting Arctic infrastructure and natural resources. *Journal of Geophysical Research: Biogeosciences*, *121*, 567–585. https://doi.org/10.1002/2015JG003125

Karaoulis, M., Revil, A., Tsourlos, P., Werkema, D. D., & Minsley, B. J. (2013). IP4DI: A software for time-lapse 2D/3D DC-resistivity and induced polarization tomography. *Computers & Geosciences*, *54*, 164–170. https://doi.org/10.1016/j.cageo.2013.01.008

Karaoulis, M., Tsourlos, P., Kim, J.-H., & Revil, A. (2014). 4D time-lapse ERT inversion: Introducing combined time and space constraints. *Near Surface Geophysics*, *12*(1), 25–34. https://doi.org/10.3997/1873-0604.2013004

Kneisel, C. (2006). Assessment of subsurface lithology in mountain environments using 2D resistivity imaging. *Geomorphology*, *80*, 32–44. https://doi.org/10.1016/j.geomorph.2005.09.012

Magnin, F., Krautblatter, M., Deline, P., Ravanel, L., Malet, E., & Bevington, A. (2015). Determination of warm, sensitive permafrost areas in near-vertical rockwalls and evaluation of distributed models by electrical resistivity tomography. *Journal of Geophysical Research: Earth Surface*, *120*, 745–762. https://doi.org/10.1002/2014JF003351

Minsley, B. J., Wellman, T. P., Walvoord, M. A., & Revil, A. (2015). Sensitivity of airborne geophysical data to sublacustrine and near-surface permafrost thaw. *The Cryosphere*, *9*(2), 781–794. https://doi.org/10.5194/tc-9-781

Moch, X., Palomares, M., Claudon, F., Souyri, B., & Stutz, B. (2015). Geothermal helical heat exchangers: Coupling with a reversible heat pump in Western Europe. *Applied Thermal Engineering*, *81*, 368–375. https://doi.org/10.1016/j.applthermaleng.2015.01.072

Ravanel, L., Magnin, F., & Deline, P. (2017). Impacts of the 2003 and 2015 summer heatwaves on permafrost-affected rock-walls in the Mont Blanc massif. *Science of the Total Environment*, *609*, 132–143. https://doi.org/10.1016/j.scitotenv.2017.07.055

Ren, Z., & Kalscheuer, T. (2019). Uncertainty and resolution analysis of 2D and 3D inversion models computed from geophysical electromagnetic data. *Surveys in Geophysics*, 1–66. https://doi.org/10.1007/s10712-019-09567-3

Sass, O. (2004). Rock moisture fluctuations during freeze-thaw cycles: Preliminary results from electrical resistivity measurements. *Polar Geography*, *28*(1), 13–31. https://doi.org/10.1080/789610157

Schaefer, K., Lantuit, H., Romanovsky, V., Schuur, A., & Witt, R. (2014). The impact of the permafrost carbon feedback on global climate. *Environmental Research Letters*, *9*(8). https://doi.org/10.1088/1748-9326/9/8/085003

Scott, W., Sellmann, P., & Hunter, J. (1990). Geophysics in the study of permafrost, in: Geotechnical and environmental geophysics, investigations in geophysics. *Society of Exploration Geophysicists*, 355–384. https://doi.org/10.1190/1.9781560802785.ch13

Self, S. J., Reddy, B. V., & Rosen, M. A. (2013). Geothermal heat pump systems: Status review and comparison with other heating options. *Applied Energy*, *101*, 341–348. https://doi.org/10.1016/j.apenergy.2012.01.048

Spans, E. J. A., & Baker, J. M. (1996). The soil freezing characteristics: Its measurement and similarity to the soil moisture characteristic. *Soil Science Society of America*, *60*, 13–19.

Vinegar, H. J., & Waxman, M. H. (1984). Induced polarization of shaly sands. *Geophysics*, *49*(8), 1267–1287.

Zimmermann, E., Kemna, A., Berwix, J., Glaas, W., Münch, H. M., & Huisman, J. A. (2008). A high-accuracy impedance spectrometer for measuring sediments with low polarizability. *Measurement Science and Technology*, *19*(10), 105603. https://doi.org/10.1088/0957-0233/19/10/105603